

# Nonlocal Homogenization Model for Wave Dispersion and Attenuation in Elastic and Viscoelastic Periodic Layered Media

**Ruize Hu**

Department of Civil and Environmental Engineering  
Vanderbilt University  
Nashville, TN 37235  
Email: ruize.hu@vanderbilt.edu

**Caglar Oskay\***

Department of Civil and Environmental Engineering  
Vanderbilt University  
Nashville, TN 37235  
Email: caglar.oskay@vanderbilt.edu

*This manuscript presents a new nonlocal homogenization model for wave dispersion and attenuation in elastic and viscoelastic periodic layered media. Homogenization with multiple spatial scales based on asymptotic expansions of up to eighth order is employed to formulate the proposed nonlocal homogenization model. A momentum balance equation, nonlocal in both space and time, is formulated consistent with the gradient elasticity theory. A key contribution in this regard is that all model coefficients including high order length-scale parameters are derived directly from microstructural material properties and geometry. The capability of the proposed model in capturing the characteristics of wave propagation in heterogeneous media is demonstrated in multiphase elastic and viscoelastic materials. The nonlocal homogenization model is shown to accurately predict wave dispersion and attenuation within the acoustic regime for both elastic and viscoelastic layered composites.*

*Keywords: Homogenization; Higher-order models; Wave propagation; Band gap; Viscoelastic composites*

## 1 Introduction

Heterogeneous materials exhibit complex response patterns when subjected to dynamic loading due to the intrinsic wave interactions induced by reflections and refractions at material constituent interfaces. Controlling these interactions offer tremendous opportunities in many engineering applications. By tailoring the constituent material properties and microstructure, heterogeneous materials with favorable properties within targeted frequency ranges, including cloaking [1, 2], energy harvesting [3, 4], vibration control [5] and impact survivability [6], could be achieved.

Band gap phenomenon, i.e., complete attenuation of waves within certain frequency ranges, has been extensively investigated over the past two decades for composite materials with periodic microstructures (i.e., phononic crystals [7, 8] and acoustic metamaterials [9, 10]). When the length of the traveling wave approaches the size of material microstructure in a composite medium, the waveform starts to interact with the microstructure through reflections and refractions at the interfaces of the constituent materials. One consequence of this interaction is dispersion, which leads to the distortion of wave shape and change of wave velocity. Another consequence is wave attenuation when the wave frequency is within stop bands. This manuscript is concerned with dispersion and wave attenuation characteristics of composites with elastic and viscoelastic phases.

Early efforts of modeling dispersion and dispersion induced phenomena in heterogeneous elastic materials can be traced back to the classical works of Mindlin [11], Achenbach and Herrmann [12] among others. Analytical solutions (e.g., matrix transfer method [13] and plane wave expansions [14]) and direct numerical simulations using finite element method [15] have been routinely employed to investigate the characteristics of wave dispersion and band gaps. As an alternative, homogenization methods have been developed over the past decades to understand and predict the overall behavior of heterogeneous materials under dynamic loads. Asymptotic homogenization pioneered by Bensoussan et al. [16] and Sanchez-Palencia [17] was employed by Boutin and Auriault [18] to investigate wave dispersion in the context of Rayleigh scattering (i.e., long wavelength regime) by exploiting the contributions from high order expansions. Noticing the secular solutions of high order expansions [19], Fish et al. [20, 21] proposed a nonlocal homogenization model that combined the momentum balance equations at the first three orders into a single macroscopic equation that captures wave dispersion in elastic composites. Andrianov et al. [22] employed the asymptotic homogenization approach to obtain the dispersion relation of elastic composites within the first Brillouin zone. Recent efforts by Hui and Oskay [23] focused on transient wave attenuation within the first band gap using a nonlocal homogenization model. By assuming harmonic wave propagation, the time dependent momentum balance equation reduces to Helmholtz equation and the steady state wave characteristics can be investigated in terms of frequency. Auriault and Boutin [24] studied the effective constitutive material properties as a function of frequency for composites with highly

---

\*Corresponding author address: VU Station B#351831, 2301 Vanderbilt Place.

contrasted constituents. The high-frequency homogenization model in Craster et al. [25] used asymptotic expansions in approximating not only the displacement field, but also the eigenfrequency of the Helmholtz equation. This model captures the dispersion curves near the edges of the first Brillouin zone. In addition to the homogenization methods based on asymptotic expansions, those that also employ Floquet-Bloch theory (e.g., [26, 27, 28, 29]) have been successful in capturing the dispersion relations of layered elastic composites.

Multiscale methods that predict transient wave propagation in finite domains have also been developed in recent years. Pham et al. [30] and Sridhar et al. [31] extended the first order computational homogenization framework to dynamic problems. The authors studied the transient response of acoustic metamaterials in two dimensions by concurrently solving a set of fully coupled macroscale and microscale balance equations. Filonova et al. [32] and Fafalis and Fish [33] investigated wave dispersion in one dimensional periodic structures using the concept of computational continua, where the quadrature rules for the numerical integration is adjusted as a function of the size scale ratio. While the above-mentioned methods show good accuracy in capturing the transient wave dispersion and attenuation, solving fully coupled momentum balance equations leads to prohibitive computational cost. Gradient elasticity modeling is an alternative approach to capture wave dispersion and band gap formation. Askes et al. [34] and Metrikine [35] studied the dispersive wave propagation using the gradient elasticity models. Dontsov et al. [36] captured the formation of the first stop band by calibrating the length-scale parameters against the analytical dispersion relation. The identification and determination of the length-scale related model parameters in multidimensional problems with inelastic materials remains outstanding [37].

Material damping provides an additional wave attenuation mechanism for composite materials with viscoelastic constituents. The effects of viscoelasticity on the band gaps of phononic crystals include shifting of the band gap frequencies, changing bandwidth, and enhancing transmission attenuation [38, 39, 40]. Modeling research of band gaps of viscoelastic composites typically focused on characterization of the band gap structure in the context of dispersion analysis [41, 42, 43], or wave transmission attenuation using direct numerical simulations [38, 39, 40]. While many homogenization approaches are proposed for elastic composites, those for viscoelastic composites are relatively rare. Auriault and Boutin [24] studied the effect of viscoelasticity on the dynamic effective material properties. Hui and Oskay [44, 45] derived a nonlocal homogenization model in the Laplace domain, which captures wave dispersion and attenuation behavior in viscoelastic composites.

In this manuscript, we propose a new nonlocal homogenization model that considers the asymptotic expansions of up to eighth order for wave propagation in periodic layered composites with elastic and viscoelastic phases. The resulting macroscopic momentum balance equation of the proposed model is of the same structure as gradient elasticity

models (e.g. [35, 34, 36]), yet all the model parameters are computed directly from the microscale equilibrium equations and dependent on the microstructural material properties and geometry. Although the concept of applying high order correctors to the first order asymptotic homogenization has been previously proposed [46, 47, 18, 48] for problems with poor separation of scales, the proposed model is unique in (1) its attempt to link the asymptotic homogenization with the gradient elasticity models and; (2) it investigates transient wave propagation and dispersion in viscoelastic materials. The performance of the proposed model is assessed by verifying the dispersion relation and transient wave propagation in elastic and viscoelastic composites against analytical solutions and direct numerical simulations.

The remainder of this manuscript is organized as follows: Section 2 presents the description of the problem and the multiscale setting. Section 3 describes the general asymptotic analysis for dynamic problems. Section 4 provides the derivation of the nonlocal homogenization model for periodic layered composites with elastic and viscoelastic constituents. Section 5 verifies the proposed model in two examples, i.e., elastic bilayer and viscoelastic four-layered microstructure. The conclusions and future research directions are provided in Section 6.

## 2 Problem setting

Consider a one-dimensional heterogeneous body with layered microstructure (e.g., 1D phononic crystals [49]). The domain of the body,  $\Omega = [0, L]$  is formed by repetition of  $m$  locally periodic microstructures,  $\Theta$ , with size  $l = L/m$ . The unit cell of the microstructure domain consists of  $N$  material phases, with the domain of phase  $j$  denoted by  $\Theta_j$ .  $x$  and  $y$  indicate the position coordinates at macro- and micro- scales, respectively, where the two coordinates are related to each other by  $y = x/\zeta$ , and  $0 < \zeta \ll 1$  is the small scaling parameter. In the context of dynamic analysis, the scaling parameter is defined as the ratio between the microstructure unit cell size and the length of deformation wave (i.e.,  $\zeta = l/\lambda$ , where  $\lambda$  is the deformation wavelength).

Consider an arbitrary response field,  $f^\zeta(x, t)$ , which oscillates in space due to fluctuations induced by material heterogeneity. A two scale spatial decomposition is applied to express the response field in terms of both macroscale and microscale coordinates,  $f^\zeta(x, t) = f(x, y(x), t)$ , where, superscript  $\zeta$  indicates the dependence of the response field on the microstructural heterogeneity. The spatial derivative of  $f^\zeta$  is obtained by applying the chain rule,  $f^\zeta_x(x, t) = f_{,x}(x, y, t) + \frac{1}{\zeta} f_{,y}(x, y, t)$ , where, subscript comma followed by  $x$  and  $y$  denote the spatial derivative with respect to the macroscale and microscale coordinates, respectively. The response fields are assumed to be spatially periodic,  $f(x, y, t) = f(x, y + \hat{l}, t)$ , where,  $\hat{l}$  denotes the period of the microstructure in the microscale coordinate (i.e.,  $\hat{l} = l/\zeta$ ). The response field of the heterogeneous body subjected to dynamic load is governed

by the momentum balance equation:

$$\sigma_{,x}^{\zeta}(x,t) = \rho^{\zeta}(x)u_{,tt}^{\zeta}(x,t) \quad (1)$$

in which,  $\sigma^{\zeta}$  and  $u^{\zeta}$  are the stress and displacement fields, respectively; and  $\rho^{\zeta}$  denotes density.

The constitutive response is described by a generalized linear viscoelastic model:

$$\sigma^{\zeta}(x,t) = \int_0^t g^{\zeta}(x,t-\tau)\varepsilon_{,\tau}^{\zeta}(x,\tau)d\tau \quad (2)$$

where,  $g^{\zeta}$  is the modulus function and  $\varepsilon^{\zeta}(x,t) = u_{,x}^{\zeta}(x,t)$  is the strain. The dissipative process within viscoelastic constituents may lead to localized heating, which in turn changes the constitutive behavior [50]. This thermal effect is not considered in the current work. Elastic behavior can be recovered by setting  $g^{\zeta}(x,t) = E^{\zeta}$ , where  $E^{\zeta}$  denotes the elastic modulus. We assume the material properties of each constituent are of the same order of magnitude.

The dynamic load is applied in the form of prescribed displacement at the boundaries:

$$u^{\zeta}(0,t) = 0; \quad u^{\zeta}(L,t) = \tilde{u}(t) \quad (3)$$

where,  $\tilde{u}(t)$  is the prescribed boundary data. The initial conditions are:

$$u^{\zeta}(x,0) = u^0(x); \quad u_{,t}^{\zeta}(x,0) = v^0(x) \quad (4)$$

where,  $u^0(x)$  and  $v^0(x)$  are the prescribed data.

The particular forms of the generalized viscoelastic constitutive model and the momentum balance equation (Eq. 1) permit a simpler description of the governing boundary value problem in the Laplace domain. We introduce the key characteristics of the Laplace transform, recast the governing system of equations, and derive the nonlocal homogenization model in the Laplace domain. By this approach, the convolution integral form of the viscoelastic constitutive relation is transformed to multiplication of strain and modulus function, which is dependent on the Laplace variable.

The Laplace transform of an arbitrary, real valued, time varying function,  $f$ , is defined as:

$$\mathcal{F}(s) \equiv \mathcal{L}(f(t)) = \int_0^{\infty} e^{-st}f(t)dt \quad (5)$$

where, the Laplace variable,  $s$ , and the transformed function in Laplace domain,  $\mathcal{F}$ , are complex valued (i.e.,  $s \in \mathbb{C}$  and  $\mathcal{F} : \mathbb{C} \rightarrow \mathbb{C}$ ). The derivative rule for the Laplace transform

is given as:

$$\mathcal{L}(f, \underbrace{tt \dots t}_{n \text{ times}}(t)) = s^n \mathcal{F}(s) - s^{n-1}f(0) - \dots - \underbrace{f, \underbrace{tt \dots t}_{n-1 \text{ times}}(0)}_{n-1 \text{ times}} \quad (6)$$

For simplicity of the derivation in Laplace domain, statically undeformed initial condition is assumed throughout this manuscript, i.e., any field variables (displacement and its derivatives) are initially zeros,  $u^0(x) = 0$  and  $v^0(x) = 0$ , thus:

$$\mathcal{L}(f, \underbrace{tt \dots t}_{n \text{ times}}(t)) = s^n \mathcal{F}(s) \quad (7)$$

The convolution integral rule is given as:

$$\mathcal{L}\left(\int_0^t f_1(t-\xi)f_2(\xi)d\xi\right) = \mathcal{L}(f_1)\mathcal{L}(f_2) \quad (8)$$

The momentum balance equation, Eq. 1, in the Laplace domain is:

$$\sigma_{,x}^{\zeta}(x,s) = \rho^{\zeta}(x)s^2u^{\zeta}(x,s) \quad (9)$$

Applying the convolution integral rule (Eq. 8) and derivative rule (Eq. 7) to the generalized linear viscoelastic model (Eq. 2), the viscoelastic constitutive relation in the Laplace domain is written as:

$$\sigma^{\zeta}(x,s) = E^{\zeta}(x,s)\varepsilon^{\zeta}(x,s) \quad (10)$$

where, the modulus function,  $E^{\zeta}(x,s)$ , in the Laplace domain is related to the modulus function in the time domain,  $g^{\zeta}$ , as  $E^{\zeta}(x,s) = s\mathcal{L}(g^{\zeta}(x,t))$ .

The boundary conditions in the Laplace domain are transformed from Eq. 3, and written as:

$$u^{\zeta}(0,s) = 0; \quad u^{\zeta}(L,s) = \hat{u}(s) \quad (11)$$

### 3 Asymptotic analysis with multiple scales

We perform a dimensional asymptotic analysis, as is frequently used in situations where only moderate contrast is present in material properties (e.g., [18, 20]). Based on the two-scale description, the displacement is approximated by the following asymptotic expansion in the Laplace domain:

$$u^{\zeta}(x,s) \equiv u(x,y,s) = u_0(x,s) + \sum_{i=1}^8 \zeta^i u_i(x,y,s) + O(\zeta^9) \quad (12)$$

where,  $u_0$  denotes the macroscopic displacement field and is dependent on the macroscale coordinate only; and  $u_i$  are high order displacement fields which are functions of both macroscale and microscale coordinates. The macroscopic nature of  $u_0$  is not an assumption, but a well-known consequence of the asymptotic analysis [20]. The strain field at any order is obtained as:

$$O(\zeta^i): \quad \varepsilon_i(x, y, s) = u_{i,x} + u_{i+1,y}; \quad i = 0, 1, \dots \quad (13)$$

Employing Eq. 13 along with the constitutive relation (Eq. 10), the stress field at each order is obtained as:

$$O(\zeta^i): \quad \sigma_i(x, y, s) = E(y, s)(u_{i,x} + u_{i+1,y}); \quad (14)$$

Substituting the expanded displacement field (Eq. 12) and the constitutive equations at various orders (Eq. 14) into the momentum balance equation (Eq. 1), and collecting terms with equal orders yield the equilibrium equations at each order of  $\zeta$ :

$$O(\zeta^{-1}): \quad \sigma_{0,y}(x, y, s) = 0 \quad (15a)$$

$$O(\zeta^i): \quad \sigma_{i,x}(x, y, s) + \sigma_{i+1,y}(x, y, s) = \rho(y)s^2 u_i(x, y, s) \quad (15b)$$

The classical homogenization models consider the two lowest order equilibrium equations (Eq. 15a and Eq. 15b with  $i = 0$ ), resulting in a macroscopic description that does not capture wave dispersion or attenuation [51, 52]. This model is valid only when the deformation wavelength is large enough that the local dispersion due to material heterogeneities is negligible. Considering additional two equations at  $O(\zeta^1)$  and  $O(\zeta^2)$ , it is possible to capture dispersive effects and wave propagation in shorter deformation wavelength scenarios [20, 22, 44].

The equilibrium equations (Eq. 15a, b) are evaluated sequentially by the decomposition of the corresponding displacement fields into macroscale components, which are independent of the microscale coordinate, and influence functions that incorporate the effect of microstructures. The following asymptotic procedure is well known and briefly explained herein since it sets the stage for the proposed nonlocal model. We start by considering the following decomposition:

$$u_1(x, y, s) = U_1(x, s) + H_1(y)U_{0,x}(x, s) \quad (16)$$

where,  $H_1(y)$  denotes the first order microscopic influence function, and  $U_1(x, s)$  is the first order macroscale displacement, and  $U_0(x, s) = u_0(x, s)$ . Combining Eqs. 14, 15a and 16 results in the linear equilibrium equation for the microscopic

influence function at  $O(\zeta^{-1})$ :

$$\{E(y, s)(1 + H_{1,y})\}_{,y} = 0 \quad (17)$$

The equilibrium equation for the N-layered unit cell is evaluated uniquely by imposing the following constraints [44]:

$$\text{Periodicity:} \quad u_1(y = 0) = u_1(y = \hat{l}); \quad (18a)$$

$$\sigma_0(y = 0) = \sigma_0(y = \hat{l})$$

$$\text{Continuity:} \quad \llbracket u_1(y = \sum_{j=1}^n \hat{l}_j) \rrbracket = 0; \quad (18b)$$

$$\llbracket \sigma_0(y = \sum_{j=1}^n \hat{l}_j) \rrbracket = 0;$$

$$n = 1, 2, \dots, N-1$$

$$\text{Normalization:} \quad \langle u_1(x, y, t) \rangle = U_1(x, t) \rightarrow \langle H_1(y) \rangle = 0 \quad (18c)$$

where,  $\hat{l}_j = l_j/\zeta$  denote the length of  $j^{\text{th}}$  layer in microscale coordinate.  $l_j$  is the physical length of the  $j^{\text{th}}$  layer.  $\llbracket \cdot \rrbracket$  denotes the jump operator and  $y = \sum_{j=1}^n \hat{l}_j$  is the location of the constituent interfaces; and  $\langle \cdot \rangle$  is defined as a spatial averaging operator over the unit cell:

$$\langle f \rangle = \frac{1}{\hat{l}} \int_0^{\hat{l}} f(x, y, s) dy \quad (19)$$

The  $O(1)$  momentum balance equation is obtained by applying the averaging operator (i.e., Eq. 19) to the corresponding equilibrium equation (Eq. 15b with  $i = 0$ ) and considering the local periodicity of  $\sigma_1(x, y, s)$ :

$$\rho_0 s^2 U_0 - E_0(s) U_{0,xx} = 0 \quad (20)$$

where,  $\rho_0$  and  $E_0(s)$  are the homogenized density and  $O(1)$  homogenized modulus, respectively:

$$\rho_0 \equiv \langle \rho \rangle = \frac{1}{\hat{l}} \sum_{j=1}^N \hat{l}_j \rho_j \quad (21)$$

$$E_0(s) = \langle E(y, s)(1 + H_{1,y}) \rangle \quad (22)$$

The procedure to evaluate influence functions and derive momentum balance equations presented above can be generalized for arbitrary orders. The recursive influence function generation process is defined in Fig. 1. This process decomposes the microscale dependent displacement  $u_i(x, y, s)$  into macroscale displacements and associated influence functions, and substitutes the decomposed displacements into equilibrium equation at  $O(\zeta^{i-2})$ . Considering the macroscale

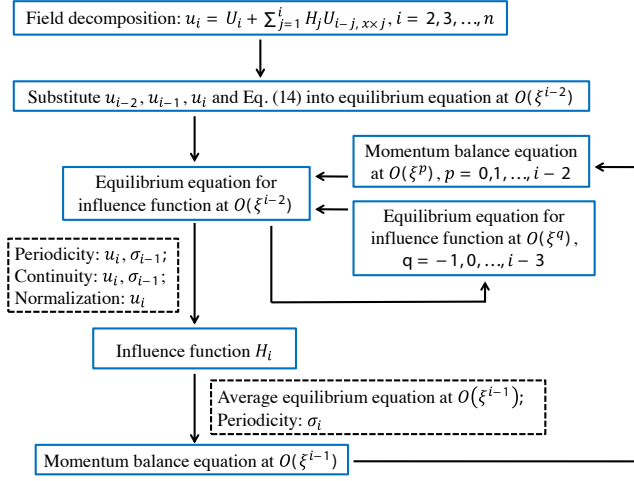


Fig. 1: Recursive influence function generation procedure.

momentum balance equations and equilibrium equations for the influence functions derived from lower orders, an equilibrium equation for influence function at  $O(\xi^{i-2})$  is obtained. By evaluating this equation with periodicity, continuity and normalization conditions, the influence function  $H_i$  is calculated. The macroscale momentum balance equation at  $O(\xi^{i-1})$  is then determined by applying the averaging operator and considering the periodicity condition of  $\sigma_i$ . Examples of deriving the influence functions and momentum balance equations can be found in [19, 20, 44].

## 4 Nonlocal homogenization model

### 4.1 Model derivation

In this section, a novel nonlocal homogenization model is proposed for elastic and viscoelastic periodic layered media. A major contribution of this model is that we explore homogenization up to  $O(\xi^6)$  and derive the momentum balance equations considering high order contributions. Furthermore, the proposed model is derived such that the momentum balance equation shares the same structure as the gradient elasticity models [35, 34, 53, 36]:

$$u_{,tt} - c_0^2 u_{,xx} + c_0^2 l_1^2 u_{,xxx} - l_2^2 u_{,xxt} + \frac{l_3^2}{c_0^2} u_{,ttt} = 0 \quad (23)$$

where  $c_0^2 = E_0/\rho_0$ . This equation has been shown to accurately capture the location and width of the first stop band, when the length scale parameters ( $l_1^2$ ,  $l_2^2$ ,  $l_3^2$ ) are calibrated against the analytical solution [36]. In contrast to the gradient elasticity models, the parameters of the nonlocal homogenization model are derived directly from the constituent material properties and microstructure.

As a result of the asymptotic analysis, the macroscale

momentum balance equations are obtained up to  $O(\xi^6)$ :

$$O(1): \quad \rho_0 s^2 U_0 - E_0(s) U_{0,xx} = 0 \quad (24a)$$

$$O(\xi^1): \quad \rho_0 s^2 U_1 - E_0(s) U_{1,xx} = 0 \quad (24b)$$

$$O(\xi^2): \quad \rho_0 s^2 U_2 - E_0(s) U_{2,xx} = \hat{E}_d(s) U_{0,xxxx} \quad (24c)$$

$$O(\xi^3): \quad \rho_0 s^2 U_3 - E_0(s) U_{3,xx} = \hat{E}_d(s) U_{1,xxxx} \quad (24d)$$

$$O(\xi^4): \quad \rho_0 s^2 U_4 - E_0(s) U_{4,xx} = \hat{E}_d(s) U_{2,xxxx} + \hat{E}_h(s) U_{0,xxxxxx} \quad (24e)$$

$$O(\xi^5): \quad \rho_0 s^2 U_5 - E_0(s) U_{5,xx} = \hat{E}_d(s) U_{3,xxxx} + \hat{E}_h(s) U_{1,xxxxxx} \quad (24f)$$

$$O(\xi^6): \quad \rho_0 s^2 U_6 - E_0(s) U_{6,xx} = \hat{E}_d(s) U_{4,xxxx} + \hat{E}_h(s) U_{2,xxxxxx} + \hat{E}_k(s) U_{0,xxxxxxx} \quad (24g)$$

where,  $U_i$  ( $i = 0, 1, \dots, 6$ ) is the macroscale displacement at  $O(\xi^i)$ ; and,  $\hat{E}_d(s)$ ,  $\hat{E}_h(s)$ ,  $\hat{E}_k(s)$  are the homogenized moduli at  $O(\xi^2)$ ,  $O(\xi^4)$ ,  $O(\xi^6)$ , respectively:

$$\hat{E}_d(s) = \langle E(y, s)(H_2 + H_{3,y}) \rangle - \langle \theta(y) E_0(s) H_2 \rangle \quad (25a)$$

$$\hat{E}_h(s) = \langle E(y, s)(H_4 + H_{5,y}) \rangle - \langle \theta(y) \hat{E}_d(s) H_2 \rangle - \langle \theta(y) E_0(s) H_4 \rangle \quad (25b)$$

$$\hat{E}_k(s) = \langle E(y, s)(H_6 + H_{7,y}) \rangle - \langle \theta(y) \hat{E}_h(s) H_2 \rangle - \langle \theta(y) \hat{E}_d(s) H_4 \rangle - \langle \theta(y) E_0(s) H_6 \rangle \quad (25c)$$

For bilayer unit cell, the analytical expressions for  $E_0$ ,  $\hat{E}_d$  and  $\hat{E}_h$  can be found in [19] and we provide  $\hat{E}_k$  in Appendix C.

The boundary conditions at each order are prescribed as:

$$BCs: U_0(0, s) = 0, \quad U_0(L, s) = \hat{u}(s) \\ U_i(0, s) = 0, \quad U_i(L, s) = 0 \quad (i = 1, 2, \dots, 6) \quad (26)$$

Under the prescribed boundary conditions, the odd order macroscale displacements are trivial (i.e.,  $U_1(x, s) = U_3(x, s) = U_5(x, s) = 0$ ). It is well known that solving Eqs. 24a, 24c, 24e, 24g sequentially at each order leads to secular solutions [19, 54]. The secularity can be eliminated by either introducing a slow temporal scale to the asymptotic analysis [54] or employing the definition of a mean displacement, which combines macroscale momentum balance equations at different orders into a single nonlocal homogenized momentum balance equation by considering the following macroscale displacement approximation [20]:

$$U^{(2n)}(x, s) = \sum_{i=0}^n \zeta^{2i} U_{2i}(x, s) + O(\zeta^{2n+2}) \quad (27)$$

where,  $U^{(2n)}$  denotes the approximation to the macroscale displacement of  $O(\zeta^{2n+2})$  accuracy.

Taking four spatial derivatives of Eq. 24a and substitut-

ing the resulting expression into Eq. 24e yields:

$$\rho_0 s^2 U_4 - E_0 U_{4,xx} = \hat{E}_d U_{2,xxxx} + \frac{\hat{E}_h}{E_0} \rho_0 s^2 U_{0,xxxx} \quad (28)$$

Inserting Eq. 24c into Eq. 28:

$$\rho_0 s^2 U_4 - E_0 U_{4,xx} = \hat{E}_d U_{2,xxxx} + \frac{\hat{E}_h \rho_0 s^2}{E_0 \hat{E}_d} (\rho_0 s^2 U_2 - E_0 U_{2,xx}) \quad (29)$$

Premultiplying Eq. 24a by  $\hat{E}_h \rho_0 s^2 / \hat{E}_d E_0$ , and adding the resulting expression to the right hand side of Eq. 24c:

$$\rho_0 s^2 U_2 - E_0 U_{2,xx} = \hat{E}_d U_{0,xxxx} + \frac{\hat{E}_h \rho_0 s^2}{E_0 \hat{E}_d} (\rho_0 s^2 U_0 - E_0 U_{0,xx}) \quad (30)$$

Premultiplying Eqs. 30 and 29 by  $\zeta^2$  and  $\zeta^4$ , respectively, adding the resulting equations to Eq. 24a, and using Eq. 27 result in:

$$\begin{aligned} & \rho_0 s^2 U^{(4)} - E_0 U_{,xx}^{(4)} - E_d U_{,xxxx}^{(4)} + \frac{E_h}{E_d} \rho_0 s^2 U_{,xx}^{(4)} - \frac{E_h}{E_0 E_d} \rho_0^2 s^4 U^{(4)} \\ &= -\zeta^6 \left( \hat{E}_d U_{4,xxxx} - \frac{\hat{E}_h}{\hat{E}_d} \rho_0 s^2 U_{4,xx} + \frac{\hat{E}_h}{E_0 \hat{E}_d} \rho_0^2 s^4 U_4 \right) \end{aligned} \quad (31)$$

where,  $E_d = \zeta^2 \hat{E}_d$  and  $E_h = \zeta^4 \hat{E}_h$  contain length scales  $l^2$  and  $l^4$ , respectively, and are computed with the physical length of the unit cell. By truncating the  $O(\zeta^6)$  perturbations in Eq. 31, we obtain the fourth order nonlocal homogenization model (NHM4):

$$\begin{aligned} \text{NHM4: } \quad & \rho_0 s^2 U - E_0 U_{,xx} - E_d U_{,xxxx} + \frac{E_h}{E_d} \rho_0 s^2 U_{,xx} \\ & - \frac{E_h}{E_0 E_d} \rho_0^2 s^4 U = 0 \end{aligned} \quad (32)$$

The superscript (4) that indicates the order of approximation is dropped for simplicity. The second order nonlocal homogenization model [44] (NHM2) and classical homogenization model (CHM) are recovered by neglecting the last two terms and last three terms on the left hand side of Eq. 32, respectively.

In order to achieve higher accuracy for shorter wave lengths, we add higher order corrections by employing Eqs. 24a-g. The procedure for obtaining the higher order equation is similar to above and aimed at achieving the structure of Eq. 23 through analysis of higher order momentum balance equations. Consider the following decomposition of

Eq. 24g:

$$\rho_0 s^2 U_6 - E_0 U_{6,xx} = \hat{E}_d U_{4,xxxx} + \hat{E}_h U_{2,xxxxxx} + \nu \hat{E}_k U_{0,xxxxxxx} + (1 - \nu) \hat{E}_k U_{0,xxxxxxx} \quad (33)$$

in which  $\nu$  is the high order correction parameter. Taking two spatial derivatives of Eq. 24e, and substituting the resulting expression for  $U_{0,xxxxxxx}$  in the third term of the right hand side of Eq. 33:

$$\begin{aligned} \rho_0 s^2 U_6 - E_0 U_{6,xx} &= \left( \hat{E}_d - \nu E_0 \frac{\hat{E}_k}{\hat{E}_h} \right) U_{4,xxxx} + \nu \frac{\hat{E}_k}{\hat{E}_h} \rho_0 s^2 U_{4,xx} \\ &+ \left( \frac{\hat{E}_h}{\hat{E}_d} - \nu \frac{\hat{E}_k}{\hat{E}_h} \right) \hat{E}_d U_{2,xxxxxx} + (1 - \nu) \hat{E}_k U_{0,xxxxxxx} \end{aligned} \quad (34)$$

Taking four spatial derivatives of Eq. 24c and substituting the resulting expression for  $U_{2,xxxxxx}$  in Eq. 34:

$$\begin{aligned} \rho_0 s^2 U_6 - E_0 U_{6,xx} &= \left( \hat{E}_d - \nu E_0 \frac{\hat{E}_k}{\hat{E}_h} \right) U_{4,xxxx} \\ &+ \nu \frac{\hat{E}_k}{\hat{E}_h} \rho_0 s^2 U_{4,xx} + \left( \frac{\hat{E}_h}{\hat{E}_d} - \nu \frac{\hat{E}_k}{\hat{E}_h} \right) \frac{\hat{E}_d}{E_0} \rho_0 s^2 U_{2,xxxx} \\ &+ \left[ (1 - \nu) \hat{E}_k - \left( \frac{\hat{E}_h}{\hat{E}_d} - \nu \frac{\hat{E}_k}{\hat{E}_h} \right) \frac{\hat{E}_d^2}{E_0} \right] U_{0,xxxxxxx} \end{aligned} \quad (35)$$

Substituting Eq. 24e for  $U_{2,xxxx}$  in Eq. 35, and taking six spatial derivatives of Eq. 24a and inserting the resulting expression for  $s^2 U_{0,xxxxxx}$ :

$$\begin{aligned} \rho_0 s^2 U_6 - E_0 U_{6,xx} &= \left( \hat{E}_d - \nu E_0 \frac{\hat{E}_k}{\hat{E}_h} \right) U_{4,xxxx} \\ &+ \left( 2\nu \frac{\hat{E}_k}{\hat{E}_h} - \frac{\hat{E}_h}{\hat{E}_d} \right) \rho_0 s^2 U_{4,xx} + \left( \frac{\hat{E}_h}{E_0 \hat{E}_d} - \nu \frac{\hat{E}_k}{E_0 \hat{E}_h} \right) \rho_0^2 s^4 U_4 \\ &+ \left[ (1 - \nu) \hat{E}_k - \left( \frac{\hat{E}_h}{E_0 \hat{E}_d} - \nu \frac{\hat{E}_k}{E_0 \hat{E}_h} \right) (\hat{E}_d^2 + E_0 \hat{E}_h) \right] U_{0,xxxxxxx} \end{aligned} \quad (36)$$

Rewriting Eq. 24e in the following form:

$$\begin{aligned} \rho_0 s^2 U_4 - E_0 U_{4,xx} &= \left( \hat{E}_d - \nu E_0 \frac{\hat{E}_k}{\hat{E}_h} \right) U_{2,xxxx} + \nu \frac{\hat{E}_k}{\hat{E}_h} \rho_0 s^2 U_{2,xx} \\ &+ \nu E_0 \frac{\hat{E}_k}{\hat{E}_h} U_{2,xxxx} - \nu \frac{\hat{E}_k}{\hat{E}_h} \rho_0 s^2 U_{2,xx} + \hat{E}_h U_{0,xxxxxx} \end{aligned} \quad (37)$$

Premultiplying Eq. 24c by  $s^2$ , replacing the resulting  $s^2 U_{0,xxxx}$  by the expression resulting from taking four spatial derivatives of Eq. 24a, and substituting the resulting expres-

sion for  $U_{0,xxxxx}$  into Eq. 37:

$$\begin{aligned} \rho_0 s^2 U_4 - E_0 U_{4,xx} &= \left( \hat{E}_d - \nu E_0 \frac{\hat{E}_k}{\hat{E}_h} \right) U_{2,xxxx} + \\ &\left( \nu \frac{\hat{E}_k}{\hat{E}_h} - \frac{\hat{E}_h}{\hat{E}_d} \right) \rho_0 s^2 U_{2,xx} + \frac{\hat{E}_h}{E_0 \hat{E}_d} \rho_0^2 s^4 U_2 \\ &+ \nu \frac{\hat{E}_k}{\hat{E}_h} \left( E_0 U_{2,xxxx} - \rho_0 s^2 U_{2,xx} \right) \end{aligned} \quad (38)$$

In view of Eq. 24a and Eq. 24c, we have:

$$\begin{aligned} E_0 U_{2,xxxx} - \rho_0 s^2 U_{2,xx} &= -\hat{E}_d U_{0,xxxxx} = \\ -\hat{E}_d \frac{\rho_0}{E_0} s^2 U_{0,xxxx} &= \frac{\rho_0}{E_0} s^2 (E_0 U_{2,xx} - \rho_0 s^2 U_2) \end{aligned} \quad (39)$$

Substituting Eq. 39 into Eq. 38:

$$\begin{aligned} \rho_0 s^2 U_4 - E_0 U_{4,xx} &= \left( \hat{E}_d - \nu E_0 \frac{\hat{E}_k}{\hat{E}_h} \right) U_{2,xxxx} \\ &+ \left( 2\nu \frac{\hat{E}_k}{\hat{E}_h} - \frac{\hat{E}_h}{\hat{E}_d} \right) \rho_0 s^2 U_{2,xx} + \left( \frac{\hat{E}_h}{E_0 \hat{E}_d} - \nu \frac{\hat{E}_k}{E_0 \hat{E}_h} \right) \rho_0^2 s^4 U_2 \end{aligned} \quad (40)$$

Considering Eq. 24a, we rewrite Eq. 24c as:

$$\begin{aligned} \rho_0 s^2 U_2 - E_0 U_{2,xx} &= \left( \hat{E}_d - \nu E_0 \frac{\hat{E}_k}{\hat{E}_h} \right) U_{0,xxxx} \\ &+ \left( 2\nu \frac{\hat{E}_k}{\hat{E}_h} - \frac{\hat{E}_h}{\hat{E}_d} \right) \rho_0 s^2 U_{0,xx} + \left( \frac{\hat{E}_h}{E_0 \hat{E}_d} - \nu \frac{\hat{E}_k}{E_0 \hat{E}_h} \right) \rho_0^2 s^4 U_0 \end{aligned} \quad (41)$$

Premultiplying Eqs. 41, 40, 36 by  $\zeta^2$ ,  $\zeta^4$  and  $\zeta^6$ , respectively, adding the resulting equations to Eq. 24a and using Eq. 27:

$$\begin{aligned} \rho_0 s^2 U^{(6)} - E_0 U_{,xx}^{(6)} &- \left( E_d - \nu E_0 \frac{E_k}{E_h} \right) U_{,xxxx}^{(6)} - \\ &\left( 2\nu \frac{E_k}{E_h} - \frac{E_h}{E_d} \right) \rho_0 s^2 U_{,xx}^{(6)} - \left( \frac{E_h}{E_0 E_d} - \nu \frac{E_k}{E_0 E_h} \right) \rho_0^2 s^4 U^{(6)} = \\ &+ \zeta^6 \left[ (1 - \nu) \hat{E}_k - \left( \frac{\hat{E}_h}{E_0 \hat{E}_d} - \nu \frac{\hat{E}_k}{E_0 \hat{E}_h} \right) (\hat{E}_d^2 + E_0 \hat{E}_h) \right] U_{0,xxxxxxx} \\ &- \zeta^8 \left[ \left( \hat{E}_d - \nu E_0 \frac{\hat{E}_k}{\hat{E}_h} \right) U_{6,xxxx} + \left( 2\nu \frac{\hat{E}_k}{\hat{E}_h} - \frac{\hat{E}_h}{\hat{E}_d} \right) \rho_0 s^2 U_{6,xx} \right. \\ &\left. + \left( \frac{\hat{E}_h}{E_0 \hat{E}_d} - \nu \frac{\hat{E}_k}{E_0 \hat{E}_h} \right) \rho_0^2 s^4 U_6 \right] \end{aligned} \quad (42)$$

where,  $E_k = \zeta^6 \hat{E}_k$  has length scale  $l^6$  and is computed with

physical length of the unit cell. We note that Eq. 42 has the same asymptotic accuracy as Eq. 32 for an arbitrarily chosen  $\nu$ , due to the presence of  $O(\zeta^6)$  term on the right hand side. In particular, when  $\nu = 0$ , the left hand side of Eq. 42 recovers Eq. 32 (i.e. NHM4). Therefore, Eq. 42 represents a one-parameter family of nonlocal homogenization models as a function of  $\nu$ .  $O(\zeta^8)$  accuracy could be achieved by setting  $\nu$  such that the coefficient of  $O(\zeta^6)$  term vanishes. The expression for the correction parameter is obtained as:

$$\nu = \frac{\hat{E}_h (\hat{E}_h^2 E_0 + \hat{E}_d^2 \hat{E}_h - E_0 \hat{E}_d \hat{E}_k)}{\hat{E}_d^3 \hat{E}_k} \quad (43)$$

By truncating the  $O(\zeta^8)$  perturbations in Eq. 42, we obtain the sixth order nonlocal homogenization model (NHM6):

$$\begin{aligned} \text{NHM6: } \rho_0 s^2 U - E_0 U_{,xx} &- \left( E_d - \nu E_0 \frac{E_k}{E_h} \right) U_{,xxxx} \\ &- \left( 2\nu \frac{E_k}{E_h} - \frac{E_h}{E_d} \right) \rho_0 s^2 U_{,xx} - \left( \frac{E_h}{E_0 E_d} - \nu \frac{E_k}{E_0 E_h} \right) \rho_0^2 s^4 U = 0 \end{aligned} \quad (44)$$

The superscript (6) is dropped hereafter.

The Laplace domain derivation presented above applies to both elastic and viscoelastic layered composites. For composites that only consist elastic phases, momentum balance equations, NHM4 and NHM6, can also be derived in time domain following a similar procedure and result in:

$$\begin{aligned} \text{NHM4: } \rho_0 U_{,tt} - E_0 U_{,xx} - E_d U_{,xxxx} &+ \frac{E_h}{E_d} \rho_0 U_{,xxtt} \\ &- \frac{E_h}{E_0 E_d} \rho_0^2 U_{,tttt} = 0 \end{aligned} \quad (45)$$

$$\begin{aligned} \text{NHM6: } \rho_0 U_{,tt} - E_0 U_{,xx} &- \left( E_d - \nu E_0 \frac{E_k}{E_h} \right) U_{,xxxx} \\ &- \left( 2\nu \frac{E_k}{E_h} - \frac{E_h}{E_d} \right) \rho_0 U_{,xxtt} - \left( \frac{E_h}{E_0 E_d} - \nu \frac{E_k}{E_0 E_h} \right) \rho_0^2 U_{,tttt} = 0 \end{aligned} \quad (46)$$

The nonlocal homogenization model, NHM6, possesses the same equation structure as the nonlocal equation (Eq. 23) of gradient elasticity models. One can easily observe the corresponding relation of  $-\left(\frac{E_d}{E_0} - \nu \frac{E_k}{E_h}\right)$  and  $l_1^2$ ,  $\left(2\nu \frac{E_k}{E_h} - \frac{E_h}{E_d}\right)$  and  $l_2^2$ ,  $-\left(\frac{E_h}{E_d} - \nu \frac{E_k}{E_h}\right)$  and  $l_3^2$ , respectively. While the latter parameters have to be calibrated in the gradient elasticity models, the former are fully determined through the homogenization process.

## 4.2 High order boundary conditions

Due to the presence of fourth order derivative term, two additional high order boundary conditions, in addition to Eq. 11, must be prescribed to solve the nonlocal momentum balance equation (Eq. 44). The choice of high order boundary conditions to solve nonlocal equations of this type has been extensively discussed in [37, 34, 55, 56, 57]. Most often the second derivatives of displacement at the boundaries are prescribed [37]. The dispersion analysis of the nonlocal homogenization model for elastic composites (Appendix A) indicates that non-physical solutions exist along with the physical ones for steady-state wave propagation. In this study, the high order boundary conditions are prescribed such that the non-physical solutions are suppressed:

$$U_{,xx}(0, s) = 0, \quad U_{,xx}(L, s) = \xi^2 \hat{u}(s), \quad \omega \leq \omega_{en} \quad (47a)$$

$$U_{,xx}(0, s) = 0, \quad U_{,xx}(L, s) = \eta^2 \hat{u}(s), \quad \omega > \omega_{en} \quad (47b)$$

where  $\xi$  and  $\eta$  are the solutions to the characteristic equations of Eq. 44 and are given in Appendix B.  $\omega_{en}$  (see Appendix A) is the frequency at end of the first stop band.

For harmonic loads, the high order boundary conditions are determined based on the loading frequency. For non-harmonic loads, a Fourier analysis of the applied load that identifies the frequency spectrum is performed apriori and the high order boundary conditions are selected based on the dominant frequency components.

An alternative approach to obtain the high order boundary conditions is by deriving the expression for  $U_{,xx}$  from lower order models. Taking two spatial derivatives of the momentum balance equation of CHM:

$$\rho_0 s^2 U_{,xx} - E_0 U_{,xxxx} = 0 \quad (48)$$

Substituting Eq. 48 into the governing equation of NHM4 (Eq.32), an approximation to the fourth order differential equation is obtained:

$$\left[ \left( \frac{E_h}{E_d} - \frac{E_d}{E_0} \right) \rho_0 s^2 - E_0 \right] U_{,xx} + \rho_0 s^2 \left( 1 - \frac{E_h}{E_0 E_d} \rho_0 s^2 \right) U = 0 \quad (49)$$

From Eq. 49, we obtain the high order boundary conditions for NHM6 (Eq. 44):

$$U_{,xx}(0, s) = 0, \quad U_{,xx}(L, s) = \frac{\rho_0 s^2 \left( \frac{E_h}{E_0 E_d} \rho_0 s^2 - 1 \right)}{\left( \frac{E_h}{E_d} - \frac{E_d}{E_0} \right) \rho_0 s^2 - E_0} \hat{u}(s) \quad (50)$$

This set of high order boundary conditions does not depend on the frequency of the applied load, which makes it more convenient for viscoelastic composites, where solving for  $\omega_{en}$  is usually non-trivial.

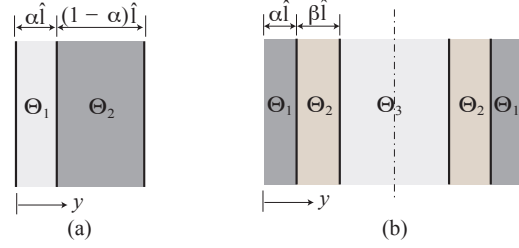


Fig. 2: Unit cell of the microstructure: (a) elastic bilayer, (b) viscoelastic four-layered.

## 5 Model verification

In this section, two examples, elastic bilayer and viscoelastic four-layered microstructures are investigated to demonstrate the capability of the proposed nonlocal homogenization model in capturing the characteristics of dispersion and transient wave propagation in periodic layered media.

### 5.1 Elastic bilayer microstructure

Consider a bilayer unit cell microstructure as illustrated in Fig. 2(a). The phases within the unit cell,  $\Theta$ , is characterized by the density, Young's modulus and length. The volume fraction of phase  $\Theta_1$  is taken as 0.5. Aluminum and steel are used for phases 1 and 2, respectively. The elastic modulus and density are 210 GPa and 7800 kg/m<sup>3</sup> for steel, and 68 GPa and 2700 kg/m<sup>3</sup> for aluminum, respectively.

#### 5.1.1 Dispersion relation

The dispersion relation of NHM6 and the mathematical description of attenuation in the stop band are provided in Appendix A. Figure 3 shows the dispersion relation of NHM6 and the reference dispersion relation (real part of the wavenumber solution is plotted). The horizontal and vertical axes are the normalized wavenumber and normalized frequency, respectively, and  $c_0$  is the homogenized wave speed (i.e.,  $c_0 = \sqrt{E_0/\rho_0}$ ). The reference dispersion relation is plotted following Bedford and Drumheller [58]. The two physical wavenumber solutions of NHM6,  $k_1$  and  $k_2$ , match with the analytical wavenumber solutions in the first pass band and second pass band, respectively. The non-physical solutions lead to negative group velocity, therefore not characteristic of wave propagation in the homogenized medium. NHM6 captures the dispersion behavior accurately in the first pass band, and the initiation and end of the first stop band, where  $kl/(2\pi) = l/\lambda = \zeta = 0.5$ , the limit of the first Brillouin zone [59]. The model starts to deviate from the reference solution as the frequency further increases and  $kl/(2\pi)$  approaches 1, where the second stop band initiates. As the scaling ratio reaches unity, the fundamental assumption of scale separation in homogenization is no longer valid [19, 60].

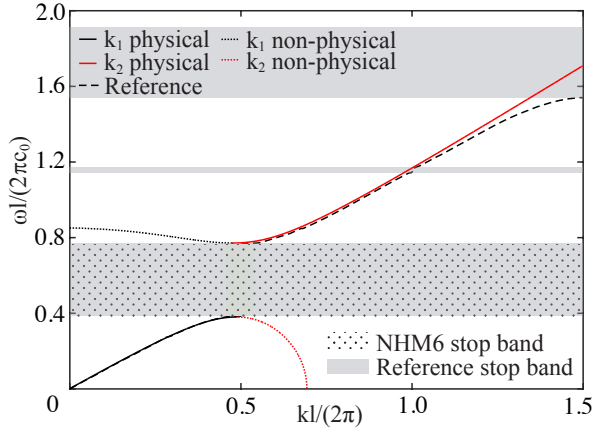


Fig. 3: Dispersion relation of NHM6 and the reference solution for bilayer microstructure.

### 5.1.2 Effect of material property contrast on model accuracy

A parametric study on the prediction error of NHM6 in terms of capturing the initiation and end of the first stop band is conducted with a large number of constituent material property combinations for the unit cell. With the material phase 1 chosen as aluminum, the material property for phase 2 is sampled in two families of materials, i.e., metals and polymers, with the material property domains  $\Omega_m = \{(E_2, \rho_2) \in \mathbb{R} \mid 100 \leq E_2 \leq 400 \text{ and } 4000 \leq \rho_2 \leq 10000\}$  and  $\Omega_p = \{(E_2, \rho_2) \in \mathbb{R} \mid 1 \leq E_2 \leq 10 \text{ and } 1000 \leq \rho_2 \leq 2000\}$ , respectively. In each of the material property domain, 100 samples are generated for  $E_2$  and  $\rho_2$ , and the prediction error is computed as  $|\omega_{NHM6} - \omega_{ref}|/\omega_{ref}$  at the stop band initiation and end frequencies for each sample. Figure 4 shows the prediction error of NHM6 for the two sets of constituent material combinations. Solid dots are the sampling points and the surface is created by quadratic fitting to the points to enhance visualization. The maximum error for stop band initiation prediction is approximately 2.5% for both Al-metal and Al-polymer microstructures. The error of stop band end prediction is relatively high compared to the initiation. In Figs. 4(b) and (d), it is noticeable that error grows as the Young's modulus ratio increases, especially for the cases which have low density ratio. The general trend of error indicates that NHM6 accurately captures the initiation of stop band for a large range of constituent material combinations. It predicts the end of the stop band reasonably well for low stiffness contrast combinations, and starts to lose accuracy for high stiffness contrast cases.

### 5.1.3 Models comparison

The capability of NHM6 in capturing the dispersion and band gap formation is due to the presence of high order terms. In order to further study the effects of the high order terms, we compare the dispersion curves of NHM6 (Eq. 46), NHM4 (Eq. 45), NHM2 and CHM in Fig. 5. While all models capture the non-dispersive wave propagation characteristics at normalized frequency of less than 0.2, CHM and

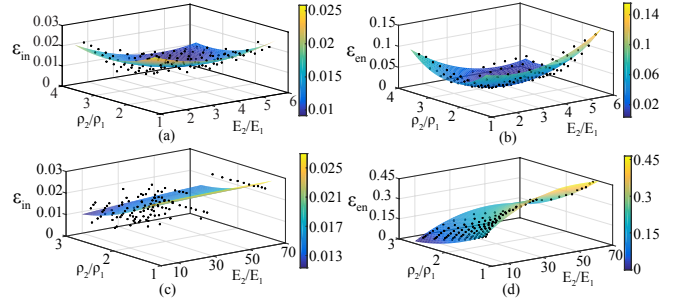


Fig. 4: Error in the prediction of the stop band. (a) Al-metal stop band initiation, (b) Al-metal stop band end, (c) Al-polymer stop band initiation, (d) Al-polymer stop band end.

NHM2 deviate from the reference dispersion relation and do not capture the band gap. NHM4 captures the dispersion up to the onset of the first stop band, but not the bandwidth. By incorporating the high order correction, NHM6 predicts the dispersion in the first and second pass band, as well as the onset and the width of the first stop band.

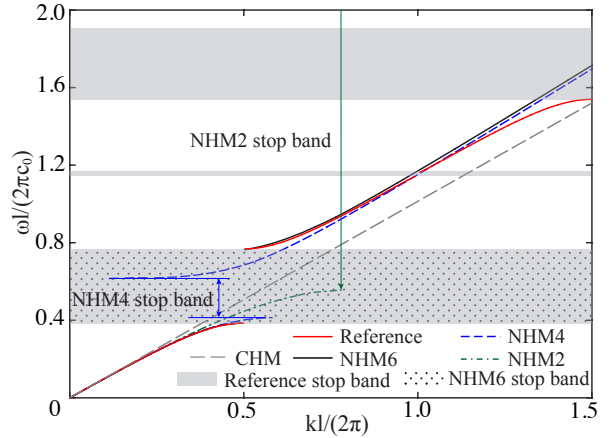


Fig. 5: Dispersion curves of NHM2, NHM4 and NHM6 compared to the reference model.

The dispersion relations of Eq. 46 and the gradient elasticity model in Eq. 23 are shown in Fig. 6 using material parameters provided in [36]. The two dispersion curves overlap with each other except the minor difference at the end of the stop band. In addition,  $O\left(\frac{E_d}{E_0} - \nu \frac{E_k}{E_h}\right) = O(l_1^2) = O(10^{-4})$ ,  $O\left(2\nu \frac{E_k}{E_h} - \frac{E_h}{E_d}\right) = O(l_2^2) = O(10^{-5})$  and  $O\left(\frac{E_h}{E_d} - \nu \frac{E_k}{E_h}\right) = O(l_3^2) = O(10^{-4})$ . The close match between the dispersion curves and the length-scale parameters indicates that the proposed model could serve as an alternative method for gradient elasticity models to determine the length-scale parameters directly from material properties and microstructures, without referring to the analytical solution, which may not be available in multidimensional problems or in the presence of viscoelastic constituents.

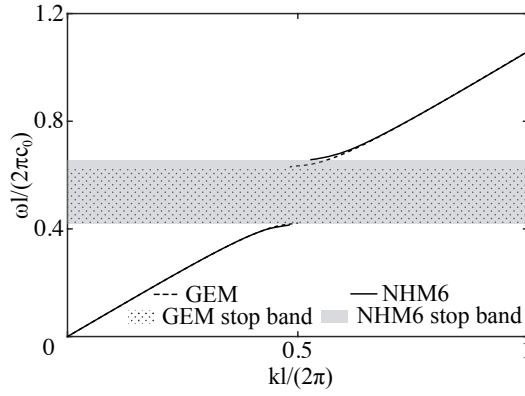


Fig. 6: Dispersion curve of NHM6 compared to the gradient elasticity model.

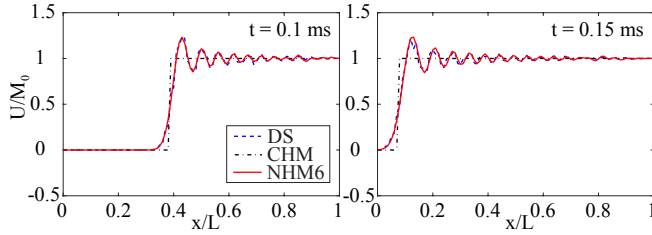


Fig. 7: Responses at two time instances under step loading: (a)  $t=0.1$  ms, (b)  $x=0.15$  ms.

#### 5.1.4 Transient wave propagation

We consider the transient response of a composite structure with aluminum-steel bilayer microstructure (see Fig. 2(a)) subjected pulse loads. The overall length of the structure is taken to be long enough,  $L = 0.5$  m, such that wave does not reflect at the fixed end within the time window of interest. The unit cell is taken to have  $l = 0.01$  m. Two pulse loads are considered, i.e., step load,  $\tilde{u}(t) = M_0 H(t)$ ,  $H(t)$  is the Heaviside function, and sinusoidal load,  $\tilde{u}(t) = M_0 \sin(2\pi ft)$ . The study compares the responses computed by NHM6, CHM and the direct solution (DS) of the original problem, where each unit cell is resolved throughout the problem domain. The time domain solution procedure for NHM6 is provided in Appendix B. The solutions for DS and CHM can be found in [44].

Figure 7 shows the normalized displacement along the layered composite at  $T = 0.1$  ms and  $T = 0.15$  ms. The responses obtained from NHM6 with high order boundary conditions, Eq. 47a, and DS both show dispersion induced phase distortion, manifested by the oscillatory behavior behind the step wave front. Due to the presence of dispersion, both NHM6 and DS have peak amplitude of  $1.2M_0$ . NHM6 shows good agreement with DS in terms of capturing the dispersive response under the prescribed step load.

Figure 8 shows the displacement histories of  $x = 0.9L$  for 0.15 ms, with the structure subjected to sinusoidal loads at frequencies 132.71 kHz and 221.18 kHz, corresponding to the normalized frequencies ( $\omega l/(2\pi c_0)$ ) of 0.3 and 0.5, respectively. At  $\omega l/(2\pi c_0) = 0.3$ , the response is in the first pass band where dispersion occurs. NHM6 predicts the dis-

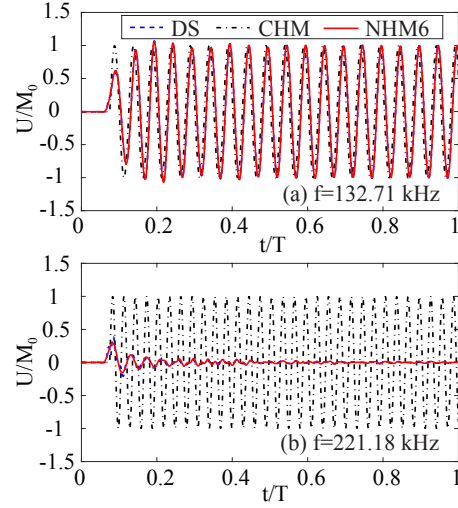


Fig. 8: Displacement histories at  $x=0.9L$  under sinusoidal loading at frequencies: (a) 132.71 kHz, (b) 221.18 kHz.

placement time history accurately compared to DS. The dispersion is manifested by the distorted phase shape of the first two cycles and slight phase shift of the dispersive models (NHM6 and DS) compared to CHM. As the frequency is increased to 221.18 kHz, the response resides in the first stop band. At this frequency, the displacement response is significantly attenuated with peak normalized amplitude of 0.25, which asymptotes to complete attenuation in time.

Figure 9 shows the maximum transmitted wave amplitude at  $x = 0.9L$  within  $t/T \in [0.5, 1]$  for sinusoidal loads at a range of frequencies  $f \in [10, 442.4]$  kHz. Solutions of NHM6 with two high order boundary conditions, i.e., Eq. 52 (BC-1) and Eq. 50 (BC-2), are compared to DS. BC-1 leads to accurate wave amplitude for frequencies within the first pass band and stop band. It starts to over predict the amplitude in the second pass band due to the increasingly poor separation of scales at high frequencies. The transmitted wave amplitude computed by BC-2 is accurate up to  $f = 120$  kHz in the first pass band and within the first stop band. As the applied loading frequency is near the initiation and end of the first stop band, the result loses accuracy.

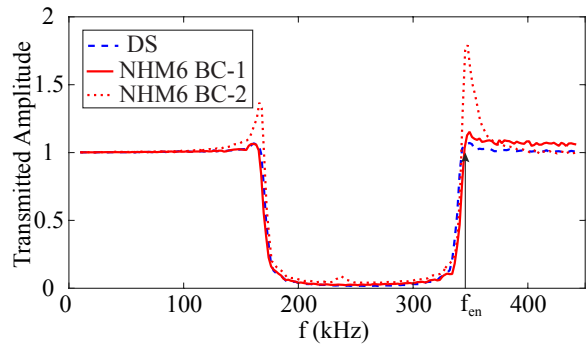


Fig. 9: Transmitted wave amplitude at  $x=0.9L$  at frequency between 10 kHz and 442.4 kHz

## 5.2 Four-layered viscoelastic microstructure

In this section, the proposed model is assessed in the context of a four-layered microstructure (see Fig. 2(b)) with both elastic and viscoelastic phases. The unit cell is composed of elastic layers, epoxy (phase 1) and rubber (phase 3), with viscoelastic layers (phase 2) inserted in between. The volume fractions of phase 1 and phase 2 are  $2\alpha$  and  $2\beta$ . In the following discussion, the volume fractions for phase 1 and phase 2 are taken as  $\alpha = 0.3$  and  $\beta = 0.1$ .

The constitutive relation of the viscoelastic phase is given by Eq. 2, where the modulus function is expressed with Prony series in time domain. After Laplace transformation, the modulus function is expressed as:

$$E_2(s) = E_\infty \left( 1 + \sum_{i=1}^n \frac{p_i s}{s + 1/q_i} \right) \quad (51)$$

where, the material properties of the viscoelastic phase is

Table 1: Material properties for elastic and viscoelastic phases.

Elastic phases			
$E_1$ [GPa]	$\rho_1$ [kg/m <sup>3</sup> ]	$E_3$ [GPa]	$\rho_3$ [kg/m <sup>3</sup> ]
1.0	1200	0.1	1100
Viscoelastic phase			
$E_\infty$ [MPa]	$\rho_2$ [kg/m <sup>3</sup> ]		
67.2	1070		
$p_1$	$p_2$	$p_3$	$p_4$
0.8458	1.686	3.594	4.342
$q_1$ [ms]	$q_2$ [ms]	$q_3$ [ms]	$q_4$ [ms]
463.4	0.06407	$1.163 \times 10^{-4}$	$7.321 \times 10^{-7}$

provided in Table 1. The sizes of the macro- and microstructures are identical to the example for the bilayer microstructure.

Figure 10 shows the transmitted wave amplitude at  $x = 0.9L$  for the four-layered viscoelastic composite structure under sinusoidal load. Loading frequency ranges from 1 to 50 kHz. Solutions obtained by NHM6 using BC-1(a), i.e., Eq. 47a, and BC-2 are compared to DS and CHM. Since the explicit expression for  $\omega_{en}$  is not available for viscoelastic microstructures, Eq. 47b is not used for high frequency loads. The wave amplitude reduction in the first pass band caused by viscoelastic dissipation, which increases monotonically as the loading frequency increases, is observed in all models. As is for elastic composite, CHM does not predict dispersion and band gap formation of viscoelastic composite. BC-1(a)

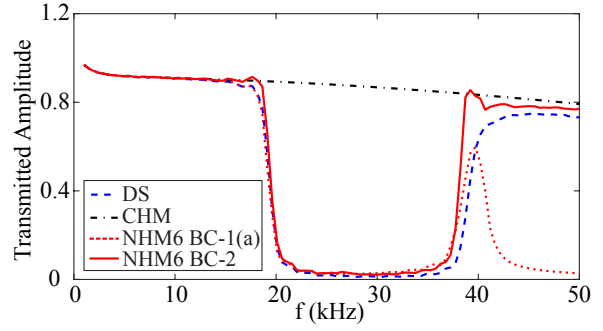


Fig. 10: Transmitted wave amplitude at  $x = 0.9L$  for the four-layered viscoelastic composite at frequency between 1 kHz and 50 kHz.

leads to accurate solution up to the end of the first stop band and deviates from the direct simulation in the second pass band. BC-2 predicts the transmitted wave amplitude up to the second pass band, except for the error near the edges of the first stop band. With BC-1(a), NHM6 captures the decreasing wave amplitude caused by dispersion in the first pass band (15-18 kHz) which is not observed in the elastic composite example (Fig. 9). The phase distortion and phase shift of the dispersive models (NHM6 with BC-1(a) and DS) in the first pass band are observed in Fig. 11(a). Within the stop band, near complete wave attenuation is present due to the combination of viscoelastic dissipation and destructive wave interactions, as is shown in Fig. 11(b).

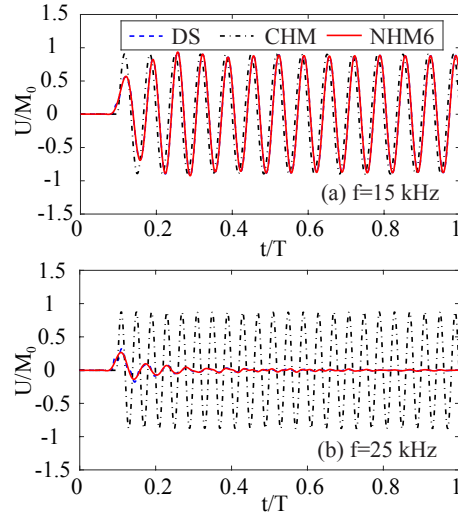


Fig. 11: Displacement histories of viscoelastic composite at  $x=0.9L$  under sinusoidal loading at frequencies: (a) 15 kHz, (b) 25 kHz.

The effect of viscoelasticity is investigated by comparing the transmitted wave amplitude for the viscoelastic composite to an elastic counterpart where the modulus function of the viscoelastic phase is replaced by its instantaneous modulus, i.e.,  $E_2(s) = E_2 = E_\infty (1 + \sum_{i=1}^n p_i)$ . As is shown in

Fig. 12, viscoelastic dissipation results in enhanced wave attenuation within the stop band, compared to the elastic case. Moreover, the first stop band of the viscoelastic composite is shifted towards lower frequency and its width becomes narrower. Similar observation was reported in [42] for one-dimensional bilayer viscoelastic phononic crystals using the plane wave expansion method.

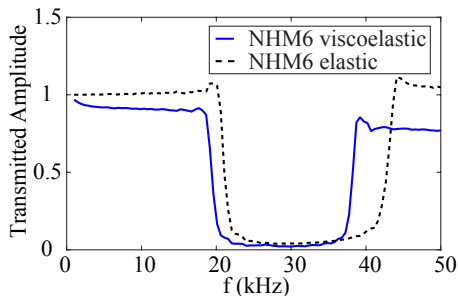


Fig. 12: Transmitted wave amplitude of elastic and viscoelastic composite computed by NHM6.

## 6 Conclusion

This manuscript presented a nonlocal homogenization model (NHM6) for the dynamic response of elastic and viscoelastic periodic layered media. The proposed model is derived based on asymptotic expansions of up to the eighth order. By introducing high order corrections, a momentum balance equation that is nonlocal in both space and time is derived. The proposed model shares the same differential equation structure as the gradient elasticity models, whereas all parameters are computed directly from the microscale boundary value problems and dependent on the material properties and microstructure only. High order boundary conditions to solve the nonlocal momentum balance equation are also discussed.

The performance of the proposed model is assessed by investigating the wave propagation characteristics in elastic bilayer and viscoelastic four-layered composite structures, and verified against analytical solutions and direct numerical simulations. NHM6 is accurate in predicting the dispersion relation of elastic wave propagation within the first pass band and the initiation and end of the first stop band for low material contrasts. The accuracy of predicting the end of the stop band decreases as the contrasts become high. In addition, NHM6 captures the transient wave dispersion and attenuation within the first pass band and stop band for elastic and viscoelastic composites. The procedure to compute model parameters of NHM6 could serve as an alternative to derive the gradient elasticity model length-scale parameters. The effect of viscoelasticity is observed to introduce viscoelastic dissipation that monotonically intensifies as the frequency increases, shift the first stop band towards lower frequency and reduce its width.

The following challenges will be addressed in the near future. First, the proposed model is developed in one-dimensional setting and it is necessary to extend NHM6 to multiple dimensions. This will naturally contribute to the applicability of NHM6 to wider range of problems with increased microstructural complexity. Second, the accuracy of the proposed model decreases as the contrasts of the phase material properties increase. Extension of the current model to account for large material property contrasts will be performed to model the dynamics of metamaterials, where the stiffness of the material phases varies by orders of magnitude.

## Acknowledgements

The authors gratefully acknowledge the financial support of the National Science Foundation, CMMI Mechanics of Materials and Structures Program, and the Computational and Data Enabled Science and Engineering (CDS&E) program (Grant No.: 1435115).

## References

- [1] Schurig, D., Mock, J. J., Justice, B. J., Cummer, S. A., Pendry, J. B., Starr, A. F., and Smith, D. R., 2006. "Metamaterial electromagnetic cloak at microwave frequencies". *Science*, **314**, pp. 977–980.
- [2] Zhang, S., Xia, C., and Fang, N., 2011. "Broadband acoustic cloak for ultrasound waves". *Phys. Rev. Lett.*, **106**, p. 024301.
- [3] Gonella, S., To, A. C., and Liu, W. K., 2009. "Interplay between phononic bandgaps and piezoelectric microstructures for energy harvesting". *J. Mech. Phys. Solids*, **57**, pp. 621–633.
- [4] Carrara, M., Cacan, M. R., Toussaint, J., Leamy, M. J., Ruzzene, M., and Erturk, A., 2013. "Metamaterial-inspired structures and concepts for elastoacoustic wave energy harvesting". *Smart Mater. Struct.*, **22**(6), p. 065004.
- [5] Naify, C. J., Chang, C. M., McKnight, G., and Nutt, S., 2011. "Transmission loss of membrane-type acoustic metamaterials with coaxial ring masses". *J. Appl. Phys.*, **110**, p. 124903.
- [6] Tan, K. T., Huang, H. H., and Sun, C. T., 2014. "Blast-wave impact mitigation using negative effective mass density concept of elastic metamaterials". *Int. J. Impact Eng.*, **64**, pp. 20–29.
- [7] Pennek, Y., Vasseur, J. O., Djafari-Rouhani, B., Dobrzyński, L., and Deymier, P. A., 2010. "Two-dimensional phononic crystals: Examples and applications". *Surf. Sci. Rep.*, **65**(8), pp. 229–291.
- [8] Hussein, M. I., Leamy, M. J., and Ruzzene, M., 2014. "Dynamics of phononic materials and structures: Historical origins, recent progress, and future outlook". *Appl. Mech. Rev.*, **66**(4), p. 040802.
- [9] Liu, Z., Zhang, X., Mao, Y., Zhu, Y. Y., Yang, Z., Chan, C. T., and Sheng, P., 2000. "Locally resonant sonic materials". *Science*, **289**, pp. 1734–1736.
- [10] Ma, G., and Sheng, P., 2016. "Acoustic metamaterials: From local resonances to broad horizons". *Sci. Adv.*, **2**(2), p. e1501595.
- [11] Mindlin, R. D., 1964. "Micro-structure in linear elasticity". *Arch. Ration. Mech. Anal.*, **16**, pp. 51–78.
- [12] Achenbach, J. D., and Herrmann, G., 1968. "Dispersion of free harmonic waves in fiber-reinforced composites". *AIAA Journal*, **6**, pp. 1832–1836.
- [13] Hussein, M. I., Hulbert, G. M., and Scott, R. A., 2006. "Dispersive elastodynamics of 1d banded materials and structures: analysis". *J. Sound Vib.*, **289**, pp. 779–806.
- [14] Sigalas, M. M., and Economou, E. N., 1992. "Elastic and acoustic wave band structure". *J. Sound Vib.*, **158**(2), pp. 377–382.
- [15] Mitchell, S. J., Pandolfi, A., and Ortiz, M., 2015. "Investigation of elastic wave transmission in a metaconcrete slab". *Mech. Mater.*, **91**, pp. 295–303.

- [16] Bensoussan, A., Lions, J.-L., and Papanicolaou, G., 1978. *Asymptotic Analysis for Periodic Structures*. North-Holland, Amsterdam.
- [17] Sanchez-Palencia, E., 1980. “Non-homogeneous media and vibration theory”. In *Non-homogeneous media and vibration theory*, Vol. 127.
- [18] Boutin, C., and Auriault, J. L., 1993. “Rayleigh scattering in elastic composite materials”. *Int. J. Eng. Sci.*, **31**, pp. 1669–1689.
- [19] Fish, J., and Chen, W., 2001. “Higher-order homogenization of initial/boundary-value problem”. *J. Eng. Mech.*, **127**, pp. 1223–1230.
- [20] Fish, J., Chen, W., and Nagai, G., 2002. “Non-local dispersive model for wave propagation in heterogeneous media: one-dimensional case”. *Int. J. Numer. Methods Eng.*, **54**(3), pp. 331–346.
- [21] Fish, J., Chen, W., and Nagai, G., 2002. “Non-local dispersive model for wave propagation in heterogeneous media: multi-dimensional case”. *Int. J. Numer. Methods Eng.*, **54**, pp. 347–363.
- [22] Andrianov, I. V., Bolshakov, V. I., Danishevskiy, V. V., and Weichert, D., 2008. “Higher order asymptotic homogenization and wave propagation in periodic composite materials”. *Proc. R. Soc. London, Ser. A*, **464**, pp. 1181–1201.
- [23] Hui, T., and Oskay, C., 2014. “A high order homogenization model for transient dynamics of heterogeneous media including micro-inertia effects”. *Comput. Methods Appl. Mech. Eng.*, **273**, pp. 181–203.
- [24] Auriault, J. L., and Boutin, C., 2012. “Long wavelength inner-resonance cut-off frequencies in elastic composite materials”. *Int. J. Solids Struct.*, **49**, pp. 3269–3281.
- [25] Craster, R. V., Kaplunov, J., and Pichugin, A. V., 2010. “High-frequency homogenization for periodic media”. *Proc. R. Soc. London, Ser. A*, **466**(2120), pp. 2341–2362.
- [26] Nemat-Nasser, S., Willis, J. R., Srivastava, A., and Amirkhizi, A. V., 2011. “Homogenization of periodic elastic composites and locally resonant sonic materials”. *Phys. Rev. B: Condens. Matter*, **83**(10), p. 104103.
- [27] Nemat-Nasser, S., and Srivastava, A., 2011. “Overall dynamic constitutive relations of layered elastic composites”. *J. Mech. Phys. Solids*, **59**(10), pp. 1953–1965.
- [28] Nassar, H., He, Q.-C., and Auffray, N., 2015. “Willis elastodynamic homogenization theory revisited for periodic media”. *J. Mech. Phys. Solids*, **77**, pp. 158–178.
- [29] Nassar, H., He, Q.-C., and Auffray, N., 2016. “On asymptotic elastodynamic homogenization approaches for periodic media”. *J. Mech. Phys. Solids*, **88**, pp. 274–290.
- [30] Pham, K., Kouznetsova, V. G., and Geers, M. G. D., 2013. “Transient computational homogenization for heterogeneous materials under dynamic excitation”. *J. Mech. Phys. Solids*, **61**(11), pp. 2125–2146.
- [31] Sridhar, A., Kouznetsova, V. G., and Geers, M. G. D., 2016. “Homogenization of locally resonant acoustic metamaterials towards an emergent enriched continuum”. *Comput. Mech.*, **57**(3), pp. 423–435.
- [32] Filonova, V., Fafalis, D., and Fish, J., 2016. “Dispersive computational continua”. *Comput. Methods Appl. Mech. Eng.*, **298**, pp. 58–79.
- [33] Fafalis, D., and Fish, J., 2015. “Computational aspects of dispersive computational continua for elastic heterogeneous media”. *Comput. Mech.*, **56**(6), pp. 931–946.
- [34] Askes, H., Metrikine, A. V., Pichugin, A. V., and Bennett, T., 2008. “Four simplified gradient elasticity models for the simulation of dispersive wave propagation”. *Philos. Mag.*, **88**, pp. 3415–3443.
- [35] Metrikine, A. V., 2006. “On causality of the gradient elasticity models”. *J. Sound Vib.*, **297**, pp. 727–742.
- [36] Dontsov, E. V., Tokmashev, R. D., and Guzina, B. B., 2013. “A physical perspective of the length scales in gradient elasticity through the prism of wave dispersion”. *Int. J. Solids Struct.*, **50**, pp. 3674–3684.
- [37] Askes, H., and Aifantis, E. C., 2011. “Gradient elasticity in statics and dynamics: an overview of formulations, length scale identification procedures, finite element implementations and new results”. *Int. J. Solids Struct.*, **48**(13), pp. 1962–1990.
- [38] Liu, Y., Yu, D., Zhao, H., Wen, J., and Wen, X., 2008. “Theoretical study of two-dimensional phononic crystals with viscoelasticity based on fractional derivative models”. *J. Phys. D: Appl. Phys.*, **41**(6), p. 065503.
- [39] Merheb, B., Deymier, P. A., Jain, M., Aleshyna-Lesuffleur, M., Mohanty, S., Berker, A., and Greger, R. W., 2008. “Elastic and viscoelastic effects in rubber/air acoustic band gap structures: A theoretical and experimental study”. *J. Appl. Phys.*, **104**(6), p. 064913.
- [40] Merheb, B., Deymier, P. A., Muralidharan, K., Bucay, J., Jain, M., Aleshyna-Lesuffleur, M., Greger, R. W., Mohanty, S., and Berker, A., 2009. “Viscoelastic effect on acoustic band gaps in polymer-fluid composites”. *Modell. Simul. Mater. Sci. Eng.*, **17**(7), p. 075013.
- [41] Hussein, M. I., and Frazier, M. J., 2010. “Band structure of phononic crystals with general damping”. *J. Appl. Phys.*, **108**(9), p. 093506.
- [42] Zhao, Y. P., and Wei, P. J., 2009. “The band gap of 1d viscoelastic phononic crystal”. *Comput. Mater. Sci.*, **46**(3), pp. 603–606.
- [43] Krushynska, A. O., Kouznetsova, V. G., and Geers, M. G. D., 2016. “Visco-elastic effects on wave dispersion in three-phase acoustic metamaterials”. *J. Mech. Phys. Solids*, **96**, pp. 29–47.
- [44] Hui, T., and Oskay, C., 2013. “A nonlocal homogenization model for wave dispersion in dissipative composite materials”. *Int. J. Solids Struct.*, **50**, pp. 38 – 48.
- [45] Hui, T., and Oskay, C., 2015. “Laplace-domain, high-order homogenization for transient dynamic response of viscoelastic composites”. *Int. J. Numer. Methods Eng.*, **103**(13), pp. 937–957.
- [46] Gambin, B., and Kröner, E., 1989. “Higher-order terms in the homogenized stress-strain relation of periodic elastic media”. *Phys. Status Solidi B*, **151**, pp. 513–519.
- [47] Smyshlyaev, V. P., and Cherednichenko, K. D., 2000. “On rigorous derivation of strain gradient effects in the overall behaviour of periodic heterogeneous media”. *J. Mech. Phys. Solids*, **48**(6), pp. 1325–1357.
- [48] Auriault, J. L., Geindreau, C., and Boutin, C., 2005. “Filtration law in porous media with poor separation of scales”. *Transp. Porous Media*, **60**(1), pp. 89–108.
- [49] El Boudouti, E. H., Djafari-Rouhani, B., Akjouj, A., and Dobrzynski, L., 2009. “Acoustic waves in solid and fluid layered materials”. *Surf. Sci. Rep.*, **64**(11), pp. 471–594.
- [50] Hu, R., Prakash, C., Tomar, V., Harr, M., Gunduz, I. E., and Oskay, C., 2016. “Experimentally-validated mesoscale modeling of the coupled mechanical–thermal response of ap–htpb energetic material under dynamic loading”. *Int. J. Fract.*, pp. 1–22.
- [51] Oskay, C., and Fish, J., 2007. “Eigendefinition-based reduced order homogenization for failure analysis of heterogeneous materials”. *Comput. Methods Appl. Mech. Eng.*, **196**, pp. 1216–1243.
- [52] Oskay, C., and Pal, G., 2009. “A multiscale failure model for analysis of thin heterogeneous plates”. *Int. J. Damage Mech.*
- [53] Pichugin, A. V., Askes, H., and Tyas, A., 2008. “Asymptotic equivalence of homogenisation procedures and fine-tuning of continuum theories”. *J. Sound Vib.*, **313**(3), pp. 858–874.
- [54] Chen, W., and Fish, J., 2001. “A dispersive model for wave propagation in periodic heterogeneous media based on homogenization with multiple spatial and temporal scales”. *J. Appl. Mech.*, **68**, pp. 153–161.
- [55] Andrianov, I. V., Awrejcewicz, J., and Weichert, D., 2009. “Improved continuous models for discrete media”. *Math. Probl. Eng.*, **2010**, p. 152.
- [56] Kaplunov, J. D., and Pichugin, A. V., 2009. *On Rational Boundary Conditions for Higher-Order Long-Wave Models*. Springer Netherlands, pp. 81–90.
- [57] Polizzotto, C., 2003. “Gradient elasticity and nonstandard boundary conditions”. *Int. J. Solids Struct.*, **40**(26), pp. 7399–7423.
- [58] Bedford, A., and Drumheller, D. S., 1994. *Elastic wave propagation*. Wiley.
- [59] Brillouin, L., 1953. *Wave propagation in periodic structures, second ed.* Dover publication.
- [60] Boutin, C., 1996. “Microstructural effects in elastic composites”. *Int. J. Solids Struct.*, **33**, pp. 1023–1051.
- [61] Brancik, L., 1999. “Programs for fast numerical inversion of laplace transforms in matlab language environment”. In *Konference MATLAB ‘99-Praha. MATLAB ‘99, Praha: Konference MATLAB ‘99, Praha*, pp. 27–39.

## Appendix A: Dispersion relations

The dispersion relation for the nonlocal homogenization model defined by Eq. 44 (NHM6) is obtained by considering a harmonic steady-state wave propagation in the homogenized medium:

$$U(x, t) = U_0 e^{i(\omega t - kx)} \quad (52)$$

where,  $U_0$  is the displacement amplitude, and  $\omega$  and  $k$  are the frequency and wavenumber, respectively. By substituting Eq. 52 into Eq. 46, the dispersion equation is obtained as:

$$\begin{aligned} (E_d - \nu E_0 \frac{E_k}{E_h}) k^4 + \left[ (2\nu \frac{E_k}{E_h} - \frac{E_h}{E_d}) \rho_0 \omega^2 - E_0 \right] k^2 \\ + \left( \frac{E_h}{E_0 E_d} - \nu \frac{E_k}{E_0 E_h} \right) \rho_0^2 \omega^4 + \rho_0 \omega^2 = 0 \end{aligned} \quad (53)$$

In general, this fourth order polynomial equation has four roots. Considering the elastic wave propagating in the positive direction:

$$\begin{aligned} k &= \sqrt{\frac{-B \pm \sqrt{B^2 - 4AC}}{2A}} \\ A &= E_d - \nu E_0 \frac{E_k}{E_h} \\ B &= (2\nu \frac{E_k}{E_h} - \frac{E_h}{E_d}) \rho_0 \omega^2 - E_0 \\ C &= \left( \frac{E_h}{E_0 E_d} - \nu \frac{E_k}{E_0 E_h} \right) \rho_0^2 \omega^4 + \rho_0 \omega^2 \end{aligned} \quad (54)$$

The wavenumber solutions for NHM4, NHM2 and CHM are obtained similarly. To seek the mathematical description of attenuation in stop bands, we rewrite the wavenumber  $k$  in the complex form,  $k = k_{re} + ik_{im}$ , where,  $k_{re}$  and  $k_{im}$  are the real part and imaginary part of wavenumber, respectively. Applying the complex wavenumber expression to the displacement solution Eq. 52, the displacement reads:

$$U(x, t) = U_0 e^{i(\omega t - k_{re}x)} e^{k_{im}x} \quad (55)$$

in which,  $e^{i(\omega t - k_{re}x)}$  contains the oscillatory feature of the displacement, while  $e^{k_{im}x}$  determines the solution to be attenuating or amplifying depending on whether  $k_{im}$  is negative or positive. Stop bands are characterized as the frequency ranges within which the elastic waves are subjected to exponential attenuation due to negative imaginary wavenumber with magnitude of strength proportional to  $|k_{im}|$ . Within the pass bands,  $k_{im} = 0$ .

The existence of complex-valued wavenumber  $k$  within the first stop band requires  $\frac{-B \pm \sqrt{B^2 - 4AC}}{2A}$  being complex, i.e.,  $y(\omega) = B^2 - 4AC < 0$ . Therefore, the initiation and end of

the first stop band are found by  $y(\omega) = B^2 - 4AC = 0$ :

$$\begin{aligned} \omega_{in} &= \sqrt{\frac{-b - \sqrt{b^2 - 4ac}}{2a}}, \quad \omega_{en} = \sqrt{\frac{-b + \sqrt{b^2 - 4ac}}{2a}} \\ a &= \rho_0^2 \left[ (2\nu \frac{E_k}{E_h} - \frac{E_h}{E_d})^2 - 4(E_d - \nu E_0 \frac{E_k}{E_h}) \left( \frac{E_h}{E_0 E_d} - \nu \frac{E_k}{E_0 E_h} \right) \right] \\ b &= -\rho_0 \left[ 2E_0 (2\nu \frac{E_k}{E_h} - \frac{E_h}{E_d}) + 4(E_d - \nu E_0 \frac{E_k}{E_h}) \right] \\ c &= E_0^2 \end{aligned} \quad (56)$$

where,  $\omega_{in}$  and  $\omega_{en}$  are the frequency that the first stop band initiates and ends, respectively.

Denote  $k_1 = \sqrt{\frac{-B - \sqrt{B^2 - 4AC}}{2A}}$  and  $k_2 = \sqrt{\frac{-B + \sqrt{B^2 - 4AC}}{2A}}$ . While  $k_1$  and  $k_2$  are both the solutions of the dispersion equation (Eq. 53), they have to be examined by physical considerations. Within the first pass band, when  $\omega = 0$ ,  $k_1 = 0$ , which recovers the result of dispersion relation of infinitely long wave, i.e.,  $k = w/c = 0$ ; on the other hand,  $k_2 = \sqrt{(E_0/A)}$ , which is not characteristic of long wave propagation. Therefore,  $k_1$  is used in the first pass band and stop band. In the second pass band, a typical observation (see Section 5.1.1) is that while  $k_2$  matches with the analytical solution well,  $k_1$  leads to negative group velocity followed by zero real wavenumber solution at higher frequencies.

## Appendix B: Time domain solution

This appendix provides the time domain solution for the nonlocal homogenization model (NHM6). The boundary value problem of NHM6 is evaluated in the Laplace domain. Time domain solution is then obtained by applying a numerical inverse Laplace transform [61]. Rewrite the nonlocal momentum balance equation (Eq. 44):

$$\begin{aligned} (E_d - \nu E_0 \frac{E_k}{E_h}) \hat{U}_{,xxxx} + \left[ \rho_0 s^2 (2\nu \frac{E_k}{E_h} - \frac{E_h}{E_d}) + E_0 \right] \hat{U}_{,xx} \\ + \left[ \rho_0^2 s^4 \left( \frac{E_h}{E_0 E_d} - \nu \frac{E_k}{E_0 E_h} \right) - \rho_0 s^2 \right] \hat{U} = 0 \end{aligned} \quad (57)$$

The fourth order differential equation is evaluated by considering the following solution form:

$$\begin{aligned} \hat{U}(x, s) = D_1(s) \sinh(\xi x) + D_2(s) \sinh(\eta x) \\ + D_3(s) \cosh(\xi x) + D_4(s) \cosh(\eta x) \end{aligned} \quad (58)$$

where  $\xi$  and  $\eta$  are the solutions of the characteristic equation of Eq. 57. With the boundary conditions Eqs. 11 and 52, the solution for frequencies in the first pass band and stop band is obtained as:

$$\hat{U}(x, s) = D_1(s) \sinh(\xi x) \quad (59)$$

and in the second pass band:

$$\hat{U}(x, s) = D_2(s) \sinh(\eta x) \quad (60)$$

The coefficients  $D_1, D_2, D_3, D_4$  are:

$$\begin{aligned} D_1(s) &= \frac{\hat{u}(s)}{\sinh(\xi L)}; & D_2(s) &= \frac{\hat{u}(s)}{\sinh(\eta L)}; \\ D_3(s) &= D_4(s) = 0 \end{aligned} \quad (61)$$

where:

$$\begin{aligned} \xi &= \sqrt{\frac{-\hat{B} + \sqrt{\hat{B}^2 - 4\hat{A}\hat{C}}}{2\hat{A}}}; & \eta &= \sqrt{\frac{-\hat{B} - \sqrt{\hat{B}^2 - 4\hat{A}\hat{C}}}{2\hat{A}}} \\ \hat{A} &= E_d - vE_0 \frac{E_k}{E_h} \\ \hat{B} &= \left(2v \frac{E_k}{E_h} - \frac{E_h}{E_d}\right) \rho_0 s^2 + E_0 \\ \hat{C} &= \left(\frac{E_h}{E_0 E_d} - v \frac{E_k}{E_0 E_h}\right) \rho_0^2 s^4 - \rho_0 s^2 \end{aligned} \quad (62)$$

### Appendix C: Analytical expression for $\hat{E}_k$

$$\begin{aligned} \hat{E}_k &= \frac{\alpha^2(1-\alpha)^2(E_1\rho_1 - E_2\rho_2)^2 E_0 \hat{l}^6}{60480\rho_0^6(E_1(1-\alpha) + \alpha E_2)^6} \left\{ \left[ (1-\alpha)^4 E_1^4 \left( \right. \right. \right. \\ &32(1-\alpha)^4 \rho_2^4 - 160\alpha(1-\alpha)^3 \rho_1 \rho_2^3 + 192\alpha^2(1-\alpha)^2 \rho_1^2 \rho_2^2 + \\ &108\alpha^3(1-\alpha) \rho_1^3 \rho_2 + 3\alpha^4 \rho_1^4 \left. \right) \left. \right. \left. \right] + \\ &\left[ \alpha(1-\alpha)^3 E_1^3 E_2 \left( -160(1-\alpha)^4 \rho_2^4 + 944\alpha(1-\alpha)^3 \rho_1 \rho_2^3 - \right. \right. \\ &1580\alpha^2(1-\alpha)^2 \rho_1^2 \rho_2^2 - 12\alpha^3(1-\alpha) \rho_1^3 \rho_2 + 108\alpha^4 \rho_1^4 \left. \right) \left. \right] + \\ &\left[ \alpha^2(1-\alpha)^2 E_1^2 E_2^2 \left( 192(1-\alpha)^4 \rho_2^4 - 1580\alpha(1-\alpha)^3 \rho_1 \rho_2^3 + \right. \right. \\ &3826\alpha^2(1-\alpha)^2 \rho_1^2 \rho_2^2 - 1580\alpha^3(1-\alpha) \rho_1^3 \rho_2 + 192\alpha^4 \rho_1^4 \left. \right) \left. \right] + \\ &\left[ \alpha^3(1-\alpha) E_1 E_2^3 \left( -160\alpha^4 \rho_1^4 + 944\alpha^3(1-\alpha) \rho_1^3 \rho_2 - \right. \right. \\ &1580\alpha^2(1-\alpha)^2 \rho_1^2 \rho_2^2 - 12\alpha(1-\alpha)^3 \rho_1 \rho_2^3 + 108(1-\alpha)^4 \rho_2^4 \left. \right) \left. \right] + \\ &\left. \left. \left. \left[ \alpha^4 E_2^4 \left( 32\alpha^4 \rho_1^4 - 160\alpha^3(1-\alpha) \rho_1^3 \rho_2 + 192\alpha^2(1-\alpha)^2 \rho_1^2 \rho_2^2 + \right. \right. \right. \right. \right. \\ &108\alpha(1-\alpha)^3 \rho_1 \rho_2^3 + 3(1-\alpha)^4 \rho_2^4 \left. \right) \left. \right. \right. \left. \right\} \end{aligned} \quad (63)$$